Environmental Science & Technology

pubs.acs.org/est

Article

Major Regional-Scale Production of O_3 and Secondary Organic Aerosol in Remote Amazon Regions from the Dynamics and Photochemistry of Urban and Forest Emissions

Janaina P. Nascimento,* Henrique M. J. Barbosa, Alessandro L. Banducci, Luciana V. Rizzo, Angel Liduvino Vara-Vela, Bruno B. Meller, Helber Gomes, André Cezar, Marco A. Franco, Milena Ponczek, Stefan Wolff, Megan M. Bela,* and Paulo Artaxo

Cite This: *Environ. Sci. Technol.* 2022, 56, 9924−9935

Read Online

ABSTRACT: The Amazon rainforest suffers increasing pressure from anthropogenic activities. A key aspect not fully understood is how anthropogenic atmospheric emissions within the basin interact with biogenic emissions and impact the forest's atmosphere and biosphere. We combine a high-resolution atmospheric chemical transport model with an improved emissions inventory and in-situ measurements to investigate a surprisingly high concentration of ozone (O_3) and secondary organic aerosol (SOA) 150−200 km downwind of Manaus city in an otherwise pristine forested region. We show that atmospheric dynamics and photochemistry determine a gross production of secondary pollutants seen in the simulation. After sunrise, the erosion of the nocturnal boundary layer mixes natural forest emissions, rich in biogenic volatile organic compounds, with a lofted pollution layer transported overnight, rich in nitrogen oxides and formaldehyde. As a result, O_3 and SOA concentrations greater than ∼47 ppbv and 1.8 $\mu g\ m^{-3}$, respectively, were found, with maximum concentrations occurring at 2 pm LT, 150−200 km downwind of Manaus city. These high concentrations affect a large primary forested area of about 11,250 km^2. These oxidative areas are under a NO*x*-limited regime so that changes in NO*x* emissions from Manaus have a significant impact on O_3 and SOA production.

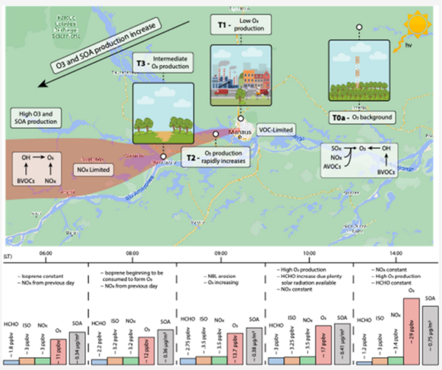

KEYWORDS: *ozone, secondary organic aerosol, atmospheric chemistry, Amazon region*

■ INTRODUCTION

The Amazon is the largest remaining tropical forest in the world. As such, biogenic volatile organic compounds (BVOCs) are emitted and found in high abundance.[1,2] The dominant BVOC emitted by the Amazon forest is isoprene, with reported ambient mixing ratios of 0.5−15 ppbv.[2] Other isoprenoids, such as monoterpenes (<1 ppbv) and sesquiterpenes (<0.16 ppbv), have also been reported.[3,4] Manaus, a city of more than 2 million people and 400.000 thousand vehicles, lies in the midst of this otherwise pristine environment. Its urban emissions make it the largest contributor of anthropogenic pollution in the Amazon basin during the wet season.[5,6] Previous studies[7,8] showed that the main contributors are light vehicles, buses, and stationary sources, such as thermal power plants and an oil refinery. This setting represents an ideal natural laboratory for investigating how anthropogenic emissions interact with biogenic compounds, modifying atmospheric chemistry and the production of ozone (O_3) and secondary organic aerosols (SOA).[9−12] Several studies have investigated how the transport of NO*x* and other anthropogenic compounds to the forest impacts the photochemical reactions that produce O_3[9,13,14] and secondary organic aerosol (SOA).[5,15,16] The Green Ocean Amazon experiment (GoAmazon2014/5), with ground and aircraft-based measurements, has shown significant changes in aerosol composition and properties in an area up to 70 km downwind from Manaus, when compared with pristine Amazonian conditions.[5,14,16,17] Experiments using an oxidation flow reactor[18] showed that additional SOA could be produced further downwind than 70 km by the interaction between biogenic precursors, such as isoprene and formaldehyde (HCHO), and available oxidants such as O_3 and hydroxyl radicals (OH). Changes in the concentration of atmospheric oxidants can affect vegetation growth rates producing leaf injury and damage to plants.[19,20] At the same time, additional SOA could impact on Earth's energy balance.[9] A substantial modification of the particle number concentration can affect

Received: February 25, 2022
Revised: June 9, 2022
Accepted: June 23, 2022
Published: July 8, 2022

the activation of cloud droplets, with possible consequences that range from suppression of cloud formation[21−25] to convective invigoration.[26,27]

Because of the relatively low biogenic emissions of nitrogen oxide (NO), the Amazon forest is generally under a NO*x*-limited O_3 production regime.[9] Therefore, when urban emissions rich in NO*x* are mixed with BVOC emissions from the forest, O_3 production is favored, and the O_3 concentration can increase considerably.[14] In contrast, the outskirts of Manaus are under a VOC-limited regime.[9] Given the high NO*x* concentrations, OH radicals are consumed by reaction with NO_2, reducing the concentration of peroxy radicals (RO2) and inhibiting O_3 production, as also observed in other urban areas.[28,29] The ratio between VOCs and NO*x* (VOC/NO*x*) combined with the maximum incremental reactivity (MIR) scale has been frequently used as an indicator of the O_3 formation regime.[11,29,30] MIR is a parameter used to quantify the contribution of VOCs to O_3 formation showing that HCHO has one of the highest O_3 yields among all VOCs.[31] According to Sillman,[12] a value of 0.28 for the ratio $HCHO/NO_Y$ ($NO_Y = NO + NO_2 + HNO_3 + PAN + NO_3 + 2N_2O_5$) usually marks the transition between the VOC-limited and NO*x*-limited regimes. As the pollution plume meanders over the forest, driven by the trade winds and river breezes, it disrupts the balance of VOCs and NO*x*, disturbing a much larger area than that of the urban environment.

Using a state-of-the-art atmospheric chemistry model with an improved emission inventory for the city of Manaus, which we developed for this study, we simulated the Amazonian atmosphere and chemistry, intending to understand how Manaus pollution impacts O_3 and SOA production. This is the first modeling study of O_3 formation during the GoAmazon2014/5 experiment. Our investigation occurs during the wet season, when urban emissions are the sole contributors of anthropogenic pollution. We focus on the "golden" week that ends on the experiment's "golden" day,[14,32] March 13, 2014. This period mainly had steady winds during the daytime, a few clouds, sunny skies, and reduced precipitation; the urban plume transported elevated gas and aerosol concentrations hundreds of kilometers downwind of Manaus. Modeled concentrations and meteorology are validated using ground and aircraft-based observations.

We show that, on average, the O_3 and SOA production peaks at 2 pm LT and ∼150−200 km downwind of Manaus (further than any previous estimates) where average concentrations are 5- and 8-fold higher, respectively, than simulations without the urban plume. Dynamics, and not only photochemistry, play a crucial role. Far from Manaus, O_3 and SOA are produced when the lofted layer of nighttime-transported anthropogenic precursors is mixed with ground emissions of BVOCs, following the early morning boundary layer development. A forested area of about 11,250 km^2 is affected by this enhanced O_3 concentration daily basis, with possible important impacts on the vegetation.[33]

■ METHODS

Code Availability. The study region was simulated with the WRF-Chem model, version 3.9.1.1[50,51] using full coupled and online meteorology, gas-phase chemistry, and aerosol and radiation feedback. Recently, a new predictive framework for Amazon forest fire smoke dispersion over South America has been developed based on WRF-Chem.[52]

WRF-Chem Setup. We used the WRF-Chem model version 3.9.1.1,[50,51] with meteorology fully coupled to aerosol and gas-phase chemistry, including feedback on radiation. The model grid covers the study region with a horizontal grid spacing of 3 km and nx = 200 and ny = 150 grid points. Vertically, hybrid sigma coordinates were used to split the atmosphere into 51 levels, the bottom 10 levels within the planetary boundary layer (PBL).

Meteorological fields from the European Centre for Medium Range Weather Forecasts (ECMWF) Reanalysis v5 (ERA5) were provided in 6 h increments with a horizontal grid spacing of 25 km, and 137 hybrid sigma pressure levels were used for the initial and boundary conditions of the meteorological variables. The chemistry initial and boundary conditions were provided by the ECMWF operational model in 3 h increments at a horizontal resolution of about 40 km × 40 km with 60 vertical levels from the surface up to 60 km. The physics, chemistry, and emission options used in this study, as well as their corresponding references, are listed in SI Appendix, Table 1. The first day was used as a spin-up period; as such, it was discarded from the analysis.

No sensitivity simulation was made regarding the aerosols feedback effects. The study region was not affected by extreme events that would necessitate a sensitivity simulation during the study period, such as large fires, which could bring a great amount of smoke plumes and consequently attenuate the radiation (e.g., Forkel et al.,[60] Kong et al.,[61] Vara-Vela et al.,[62] Liu et al.[63])

Study Area. The study area and the distribution of surrounding anthropogenic emission source and surface sites are described in detail in the study of Nascimento et al.[16] The geographical positions of the sampling stations used for the validation of the modeling in this investigation are presented in SI Appendix, Table 3. The study area with the sampling stations can be seen in the abstract graphic.

Observational Data. We used in situ measurements from several GoAmazon2014/5 surface sites.[32] At the ATTO site, the O_3 and NO*x* mixing ratios were measured using a 49i O_3 Analyzer (Thermo Environment) and Eco physics CLD TR, respectively. At the T3 site, organic and inorganic submicron aerosol mass loadings were measured with a time-of-flight aerosol mass spectrometer (ToF-AMS).[5] Mixing ratios of O_3 and CO were obtained with a 49i O_3 Analyzer (Thermo Environment) and a N_2O/CO analyzer (Los Gatos Research - LGR). Meteorological observations were made with a Vaisala WXT520 metstation, and PBL heights were measured using a ceilometer and Lidar.[39] Observed data were averaged at 1 h intervals for comparison with WRF-Chem output. Standard temperature and pressure (STP) corrections were applied to all measurements.

Measurements on-board the DoE Gulfstream 1 (G-1)[10,14] aircraft were also used. Measurements of VOC species, O_3, and CO were made with an Ionicon quadrupole high-sensitivity proton-transfer-reaction mass spectrometer (PTR-MS), a Thermo Scientific Model 49i O_3 analyzer based on measurement of UV absorption at 254 nm, and a Los Gatos Research $CO-N_2O-H_2O$ analyzer, respectively. Tropospheric (below 3 km) O_3 satellite data were obtained from previous studies[53,54] by the combination of the infrared atmospheric sounding interferometer (IASI) thermal infrared data with the global ozone monitoring experiment-2 (GOME-2) ultraviolet measurements.

https://doi.org/10.1021/acs.est.2c01358
Environ. Sci. Technol. 2022, 56, 9924−9935

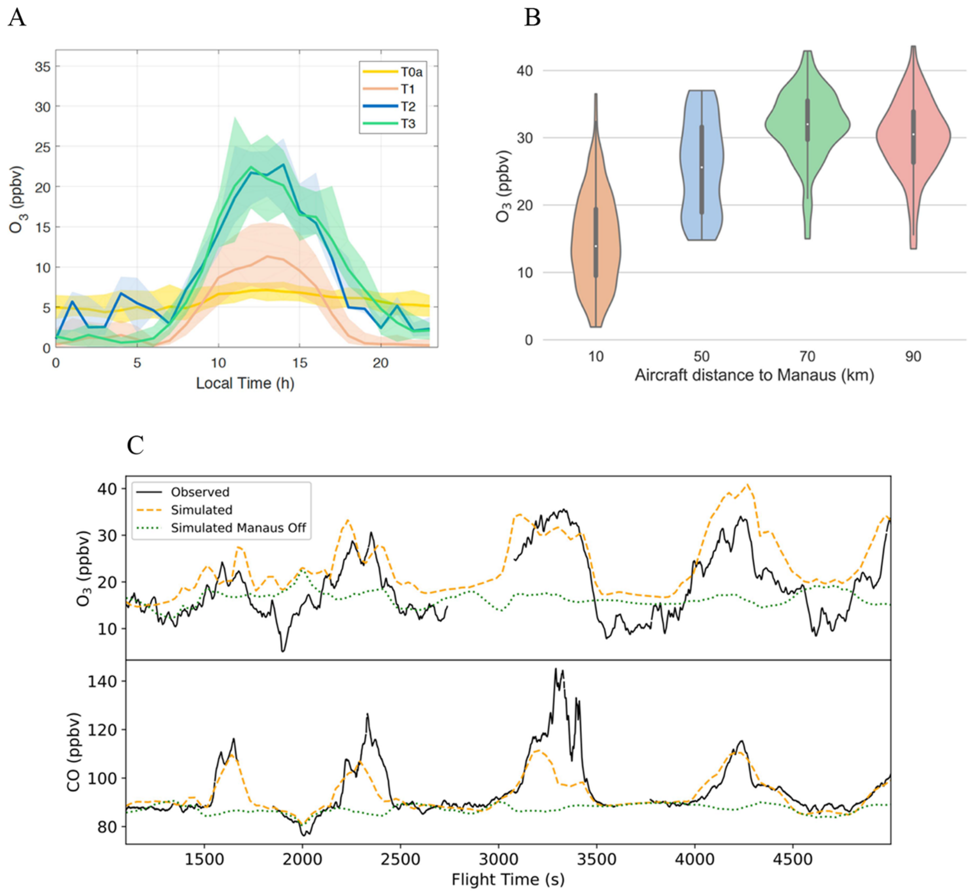

Figure 1. Observational O_3 and CO measurements in the central Amazon region. (A) Daily median O_3 profile from February to March (wet season) at the T0a site during 2014 (yellow line), the T1 site during 2016 (red line), the T2 site during 2014 (blue line), and the T3 site during 2014 (green line). The shaded areas show the 25th to 75th percentiles of the respective median lines. At the T2 and T3 sites, the O_3 values were selected by Manaus urban plume events (Methods). (B) Violin plots showing G1 aircraft measurements of O_3 at various distances from Manaus at ca. 500 m altitude on March 13, 2014. (C) G1 aircraft measurements of O_3 (top) and CO (bottom) in the Manaus pollution plume at ca. 500 m altitude compared to simulations with (orange) and without (green) Manaus emissions on March 13, 2014. The G1 Flight time is between 10:12 and 11:30 LT.

Anthropogenic Emissions. Two different inventories[7,8] were used to create the anthropogenic emission fields used in the simulations. The inventory developed by[8] includes the contributions of fixed (refinery and thermoelectric) and mobile sources, while the inventory from[7] is focused only on mobile sources. Analyses of the contributions of each source and the emission factors of the chemical species given by the inventories along with comparisons of observed data with simulations carried out using these inventories led us to reduce the VOC emissions of the Issac Sabbá (REMAN) refinery and power plants in the area given by[8] by a factor of 10. From these inventories, and our analysis, we generated emissions fields that produced satisfactory results for the representation of VOCs (acetaldehyde (CCHO), toluene (TOL Appendix, Figure S20)), as well as gaseous chemical compounds such as CO and NO*x*. These emissions fields ultimately led to the successful representation of secondary compounds such as O_3 and SOA.

Biogenic Emissions. Biogenic emissions were calculated online using the model of emissions of gases and aerosols from nature (MEGAN) version 2.[55] Based on the driving variables such as ambient temperature, solar radiation, leaf area index, and plant functional types, this model estimates the net terrestrial biosphere emission rates for different trace gases and aerosols with a global coverage at ~1 km^2 spatial resolution.

O_3 Variation Region. The scatter plots in Figures 2C−F and 4A, B show the simulated mixing ratios (with anthropogenic emissions turned on) in grid squares where the difference in HCHO or NO*y* between simulations with anthropogenic emissions on and off (On−Off) is greater than three standard deviations above the mean. The regions selected by this criterion are the most significant in O_3 production and consumption (Figure 2A, B).

Analysis Regions. To understand the mechanisms of O_3 production and how they are affected by the anthropogenic emissions, we analyzed areas around Manaus that presented different VOC and NO*x* regimes. Particularly, the *boom* region corresponds to the area most affected by the urban emissions and where the highest maximum daily concentration of O_3 is typically found, as seen in Figure 2F. It is a forest area downwind of the T3 site and comprises 11,250 km^2 (−60.75 to 565 62.29 Lon and −3.82 to −3.06 Lat). Averaging over this region was used to create Figure 3A−D.

HYSPLIT Trajectory Analysis. To calculate the transport time of polluted air masses over the forest, NOAA's hybrid single-particle Lagrangian integrated trajectory (HYSPLIT) model[56,57] was used. Simulations with HYSPLIT were driven

https://doi.org/10.1021/acs.est.2c01358
Environ. Sci. Technol. 2022, 56, 9924−9935

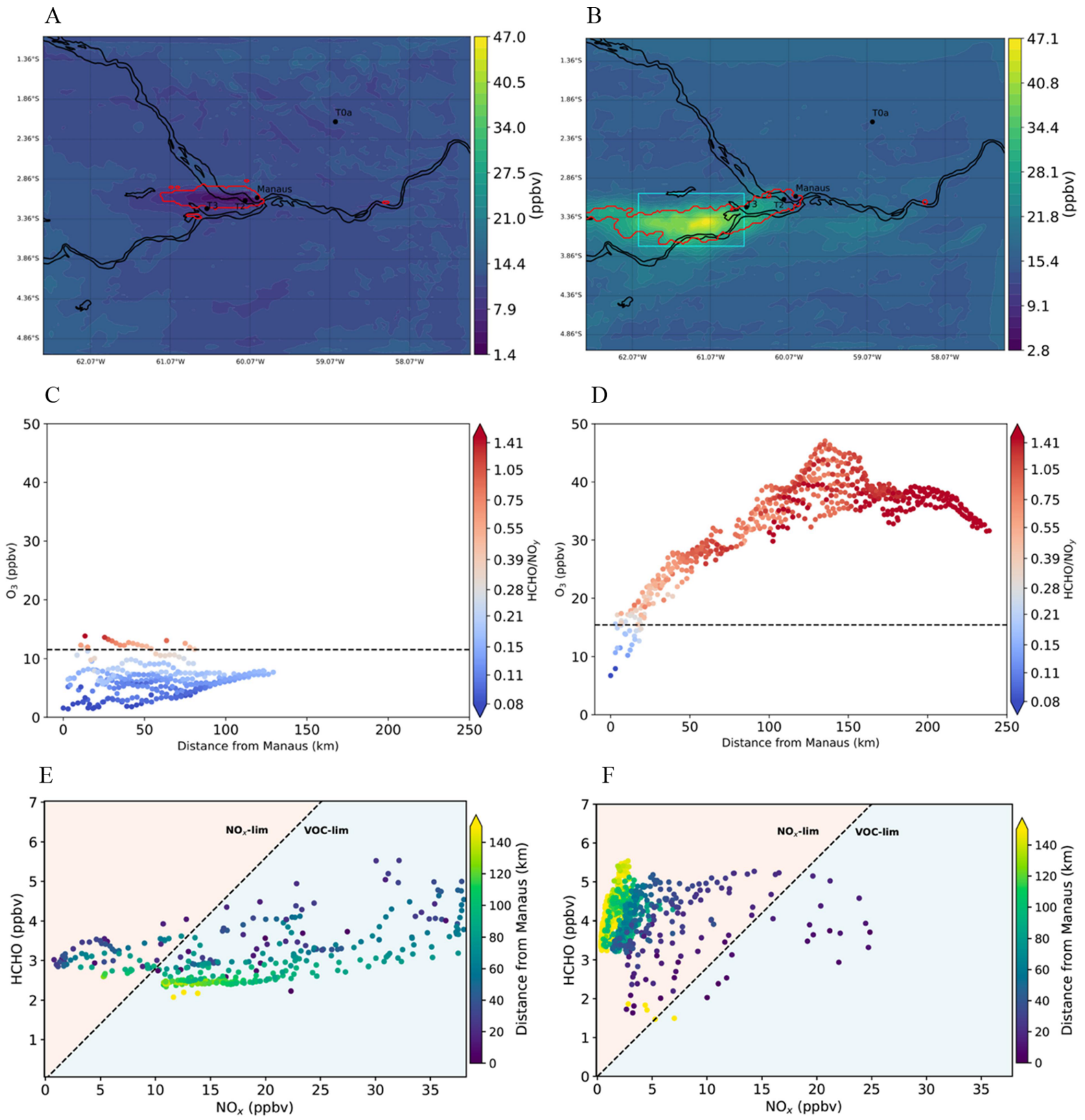

Figure 2. WRF-Chem simulated data from 8:00 (left column) and 14:00 (right column) (LT). (A,B) O_3 spatial distributions at 8:00 and 14:00 (LT) averaged daily between 9 and 14 March, 2014 and averaged between 200 and 500 m above the surface. The red line shows the O_3 variation region, the area where O_3 production is affected by urban emission plumes (see Methods). This area is also where the points for scatter plots (C–F) are drawn from. The cyan square represents the *boom* region (see Methods). (C, D) scatter plots of the O_3 mixing ratio, distance from Manaus, and O_3 production regime within the O_3 variation region at 8:00 and 14:00 (LT) averaged daily between 9 and 14 March, 2014, and averaged between 200 and 500 m above the surface. The black dashed line represents the average background values in the same area from a simulation with urban emissions turned off. (E, F) Scatter plots of the HCHO and NO*x* mixing ratios and distance from Manaus under the same selection and averaging conditions as scatter plots (C, D). Dashed line represents the O_3 production regime threshold of HCHO/NO*x* = 0.28 (see Methods).

by the meteorological fields from our WRF-Chem simulations (3 km horizontal grid spacing). Forward trajectories were integrated for 24 h with a 1 h time step, starting every hour from 8:00 LT on March 9, 2014 to 19:00 LT on March 13, 2014. For each start time, an ensemble of 40 trajectories were followed, with starting positions in the metropolitan area of Manaus, and initial heights between 100 m and 500 m above the ground level. These 4800 trajectories were used to compute the density of polluted air masses for different locations in the surroundings of Manaus (SI Appendix, Figure S11A). We divided the study domain into a rectangular grid with 0.2° horizontal spacing and counted how many trajectories crossed each grid cell. The density was defined as the ratio of the number of trajectories at a given location divided by the total number of simulated trajectories. The travel time map (SI Appendix, Figure S6A) was computed as the average of the time needed for trajectories to reach a given location, which does not vary significantly throughout the day. To understand the origin of different air masses contributing to the maximum O_3 mixing ratio around 14:00 LT, we selected those trajectories arriving between 14:00 and 18:00 h UTC (10:00−14:00 h LT) at a particular location. For this subset, we calculated the average trajectory departure time from Manaus (SI Appendix, Figure S6B), as well as the shortwave radiation, daytime hours, and cumulative precipitation along the trajectories, between the departure and arrival hours (SI Appendix, Figures S11B, S18 and S19).

https://doi.org/10.1021/acs.est.2c01358
Environ. Sci. Technol. 2022, 56, 9924−9935

Manaus Urban Plume Event Criteria. In-situ ground measurements at the GoAmazon sites T0a, T1, T2 and T3 were used to investigate the impact of the urban plume on O_3 at different distances from Manaus (Figure 1A). T0a was assumed to be always outside the plume, while T1 was always inside. At T2, in-plume time was determined based on the wind direction and speed, following a previous study[17] while the urban plume index of Thalman[58] was used at T3. Periods with precipitation between T1 and T3 were excluded.

RESULTS AND DISCUSSION

Ozone Spatial Distribution Downwind of Manaus and Model Validation. Ground-based and aircraft measurements of O_3 inside and outside the Manaus plume clearly show the impact of the urban pollution on O_3 production (Figure 1A−C). In downtown Manaus (T1 site), the O_3 mixing ratio is low despite the high concentration of precursors. The average diurnal O3 peak reaches 10ppbv, only slightly above background conditions during the GoAmazon2014/15 campaign (T0a site, averaged O_3 of 7 ± 2 ppbv) (Figure 1A) and previous experiments (T0z site, 8.5 ± 1.9 ppbv).[34] The low O_3 production at the T1 site is due to high NO*x* levels, which quickly react with OH radicals (NO*x* + OH → HNO_3). This depletion of OH through HNO_3 formation results in a decrease in the availability of RO_2, thus causing a decline in O_3 formation. As a consequence, Manaus and its surroundings are in a VOC-limited O_3 production regime.

As one moves downwind of Manaus, the dilution and mixing of primary and secondary pollutants with the BVOC-rich forest environment shift the VOC/NO*x* equilibrium, favoring O_3 production. Just 14 km downwind (T2 site, across the Negro river), the O_3 production is higher, and maximum daily O_3 concentration reaches ∼21 ppbv (16−27 ppbv minimum and maximum). Further away, at the T3 site 70 km downwind of Manaus, the values are similar to those at T2, ∼20 ppbv (16−28 ppbv minimum and maximum). In all sites, nighttime in-plume mixing ratios are much lower (1−2 ppbv) than background values (5 ppbv), as NO_2 quickly react with O_3.

A similar picture is seen in the aircraft data (for distances <90 km downwind of Manaus). Figure 1B shows how measured O_3 concentrations vary with the distance from Manaus, increasing from ∼14 ppbv over T2 (10 km downwind) to ∼32 ppbv over T3 (70 km downwind of Manaus). Similar values of O_3 were found at the ground level (SI Appendix, Figure S2), showing how well mixed the Amazon boundary layer is during the day. Differences between the in-plume and background concentrations are statistically significant (Figure 1C), indicating that Manaus' urban pollution is responsible for these changes in O_3 chemistry, in agreement with the previous studies.[5,9] Moreover, all sites present almost simultaneous high O_3 values, when solar radiation peaks (∼12−1 pm LT), suggesting that the O_3 found around T2 and T3 is produced locally, and not transported from upwind.

To investigate the underlying mechanisms of O_3 formation, WRF-Chem simulations were performed with an improved urban emissions inventory (see Methods). The model allows us to directly assess the plume's impact by contrasting simulations with and without the anthropogenic emissions and also to look at the impacts of the Manaus urban plume beyond the region measured by the aircraft and ground stations.

Figure 1C shows the excellent agreement between the observed and simulated O_3 and CO mixing ratios, following the aircraft flight transects at ∼500 m altitude on March 13 (a similar agreement is found on other days where flights occurred). At the ground level, simulated O_3 concentrations and boundary layer heights also agree well with observations (SI Appendix, Figures S1 and S2), showing that the simulations correctly captured both the downwind dispersion of the plume and the production of O_3 during the transport. The maximum O_3 mixing ratio occurs ∼150 km downwind of Manaus in approximately the same location shown by the simulations (Figure 2F). These results represent a great improvement over previous modeling studies,[13,35] demonstrating that the model can simulate the atmospheric chemistry and boundary layer processes.

Ozone Production Regimes. Figure 2A,B shows how the simulated O_3 mixing ratio varies as a function of Manaus distance in areas influenced by the pollution plume (Methods). The region close to Manaus (<25 km from the city center) is always VOC-limited because of high NO*x* emissions that sustain high NO*y* concentrations even during the daytime (Figure 2A−D). There are not enough VOCs in such areas to generate the radicals needed to convert NO to NO_2, thus suppressing O_3 production.[9,16,28] In regions downwind of Manaus (50−200 km), the O_3 production regime varies through the day, following the dispersion of precursors and the emission of BVOCs, which depend on solar radiation and temperature.[2]

The average calculated HCHO/NO*y* ratio increases from 0.27 to 3.48 between 8:00 and 14:00 LT, influenced by the increase in HCHO (0.7 ppbv) and decrease in NO*y* (20.5 ppbv) mixing ratios (Figure 2C, D). HCHO increases during the day because it is produced by the oxidation of BVOCs emitted by the forest during the daytime[2,36−38] and directly emitted by vehicular emissions in Manaus.[8] Conversely, NO*y* decreases because it is consumed in the production of O_3 and diluted by mixing with unpolluted air. However, the NO*x* mixing ratios are still much larger inside the plume than outside (∼0.02 ppbv).

Our simulations show that because of the continuous transport of NO*x*, the Manaus plume impacts O_3 mixing ratios during the whole day over a large area (11,250 km^2), with an excess consumption from 20−7 LT and excess production from 10-16 h LT (Figure 2E, F). The simulated O_3 production increases sharply after 10 LT, and the maximum mixing ratio occurs around 14 LT, ∼150−200 km downwind of Manaus. A region of high O_3 is found in satellite observations at (∼10:00 LT) during the wet seasons of 2018−2020 (SI Appendix, Figure S3), consistent with the increase in simulated O_3 at 10 LT mentioned above. The SOA mixing ratio also peaks at 14 LT at the same location (SI Appendix, Figure S4). It is important to mention that, on all simulated days, there are areas ca. 140 km from Manaus, within the *boom* region where O_3 values at 14:00 (LT) are greater than ∼47 ppbv (SI Appendix, Figure S5). Day-to-day variations show that O_3 concentrations even reach values higher than ∼50 ppbv at some times and locations. The contribution of NO*x* emitted by Manaus, although small, is sufficient to massively enhance O_3 formation at these distances. Next, we discuss how the interplay of chemistry and dynamics explain these results.

Interpreting the O_3 Production Mechanism. Pollutants from Manaus are spread to regions downwind and mixed with other compounds in the atmosphere. In order to investigate

https://doi.org/10.1021/acs.est.2c01358
Environ. Sci. Technol. 2022, 56, 9924−9935

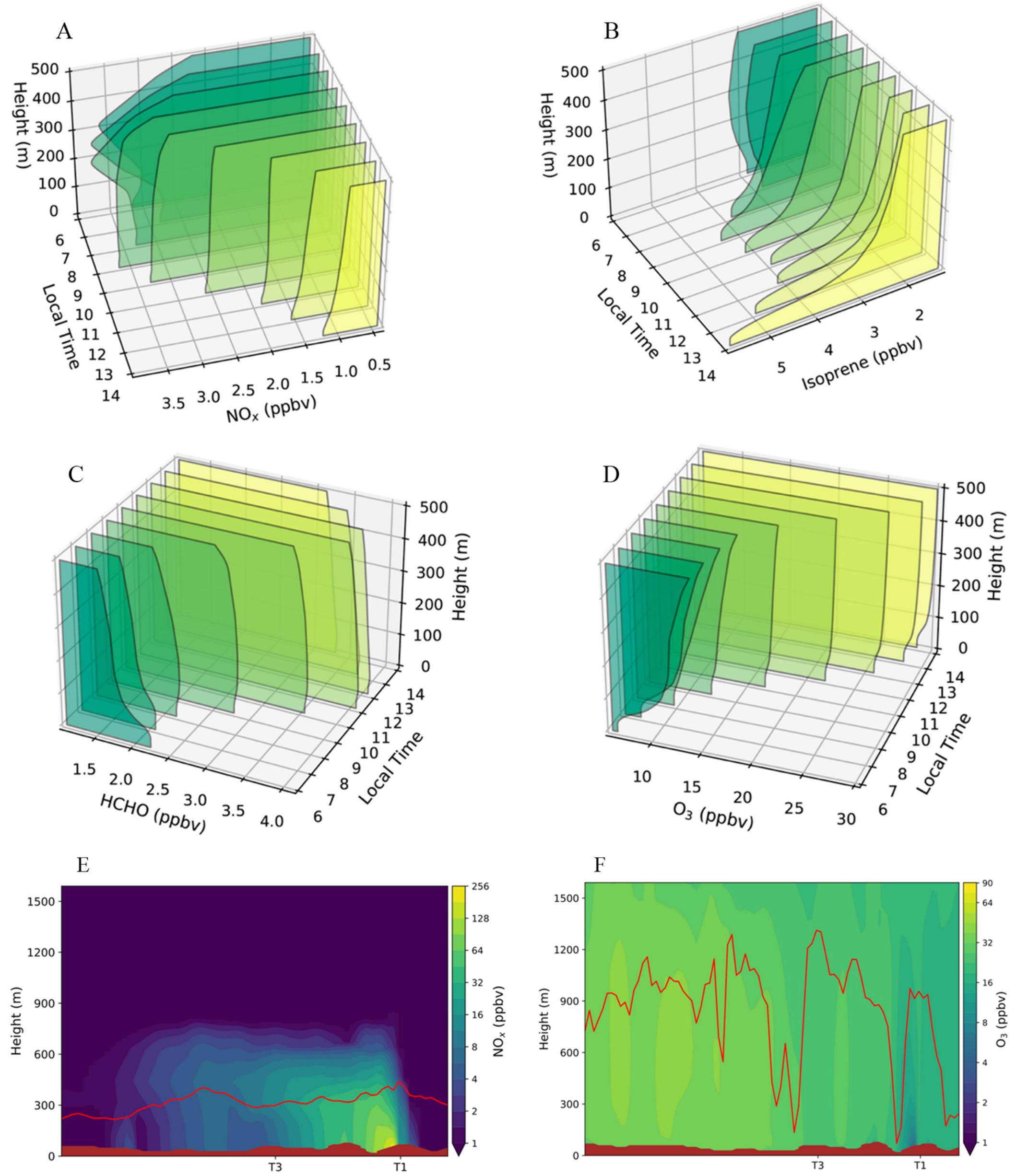

Figure 3. WRF-Chem simulated mixing ratios of NO*x* (A), isoprene (B), HCHO (C), and O_3 (D) during the daytime (6:00−14:00 LT) averaged between 9−14 March, 2014 and calculated inside the *boom* region. (E, F) Vertical cross-section of mixing ratios along the line intersecting T1 and T3 for NO*x* at 8:00 LT (E) and O_3 at 14:00 LT (F) with the PBL height represented by the red line. The brown area on the bottom is the ground.

the reasons for the peak in O_3 production ∼150−200 km away from Manaus, we analyzed chemical and dynamical processes that contribute to O_3 production. First, we estimated the time required for the Manaus plume to reach this region (see Methods). We found this to be 7.2 ± 2.9 h on average (SI Appendix, Figure S6A), without large variations during the day. Polluted air masses arriving at the *boom* region between 10 and 14 LT left Manaus before dawn, between 3 and 7 h LT, and traveled partially without sunlight. Moreover, because the nocturnal boundary layer (NBL) is quite low and stable, the pollution plume travels as a layer 300 m above the ground with minimal mixing with surface-level biogenic emissions (Figure 3E). Thus, despite pollutants being continuously blown away from Manaus, the morning rush-hour emission peak (5−7 h LT[7,8]) contributes greatly to the pollutants available to enhance O_3 production in this distant region beginning at 10 LT.

Figure 3A−D shows the hourly (6 to 14 LT) simulated vertical profiles of NO*x*, O_3, isoprene, and HCHO, all averaged over the *boom* region (Methods). Our results show that the NBL is entirely eroded by about 8−9 h LT (notice the NO*x* profile in Figure 3A), which agrees well with observations.[39] The NBL erosion increases the rate of O_3 precursor mixing in the atmosphere, bringing the NO*x* layer downward (raising NO*x* concentrations below 200 m to ∼3.5 ppbv), to meet the forest's increasing isoprene emissions at the surface. It is important to mention the nocturnal survival of isoprene (∼3 ppbv along the vertical profile 0−1000 m) (SI Appendix, Figure S7A,B), which helps the O_3 and SOA production during the early morning with the development of the planetary boundary layer (PBL). The nighttime isoprene in low-NO*x* emissions regions with high biogenic emissions were reported as an important source of VOCs on the formation of upper tropospheric organic aerosol.[40]

https://doi.org/10.1021/acs.est.2c01358
Environ. Sci. Technol. 2022, 56, 9924−9935

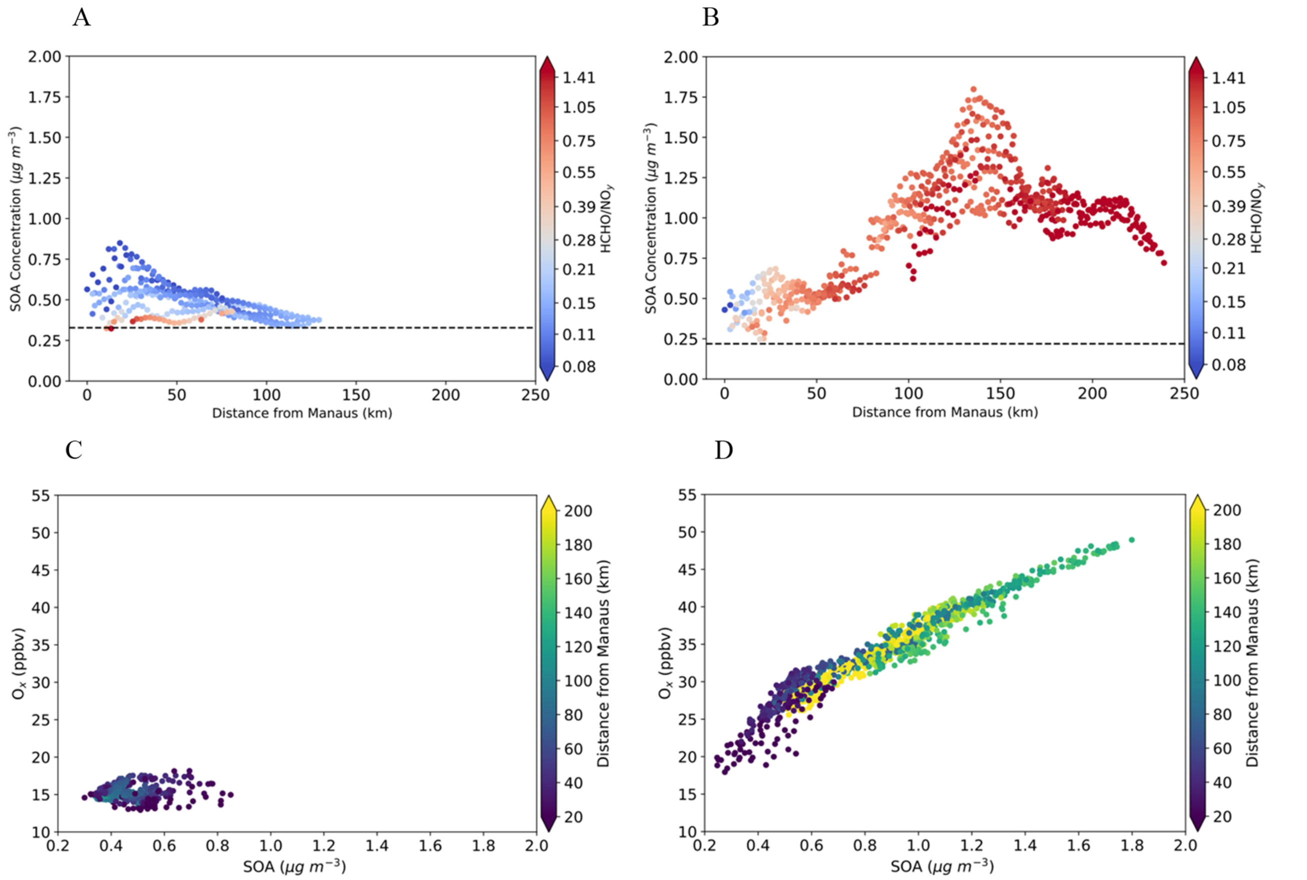

Figure 4. WRF-Chem simulated concentrations of O*x* and SOA at 8:00 (left column) and 14:00 (right column) (LT). (A, B) Scatter plots of the SOA concentration and distance from Manaus averaged each hour between 9 and 14 March, 2014, and over 200−500 m altitude. The black dashed line represents the average background values in the same area from a simulation with urban emissions turned off. (C, D) Scatter plots showing the correlations between O*x* and SOA mixing ratios and distance from Manaus averaged between 9 and 14 March, 2014 and over 200−500 m altitude.

There is a minor contribution to the available NO*x* from the nighttime storage of NO*x* oxidation products.[41,42] In the early morning, N_2O_5 and NO_3 are rapidly photolyzed, adding <0.01 ppbv of NO*x* (SI Appendix, Figure S8A,B). Figure 3B shows how the emission of isoprene surpasses its consumption, with the isoprene mixing ratios in the atmosphere increasing rapidly at the surface (4 to 6 ppbv, from 10:00 to 14:00 LT). NO*x* concentrations are significant only in the urban environment (37 to 34 ppbv); their concentrations decrease rapidly downwind through consumption and dilution (3.3 to 1.2 ppbv, from 10:00 to 14:00 LT) but are still much higher than those found in clean forest areas, where values are around 0.02 ppbv (SI Appendix, Figure S9B). The O_3 concentration reaches a maximum around 14:00 (LT), 2 h after the maximum solar radiation (SI Appendix, Figure S10). At this time, the boundary layer is fully developed, and high O_3 concentrations are found up to 110 km beyond the T3 site (Figure 3F).

The production of O_3 depends on the photolysis of precursors, and hence, there is not only a delay relative to the local solar maximum but also a dependence on the exposure of the polluted air-masses to solar radiation.[59] From our trajectory analyses (Methods), we calculated the accumulated shortwave radiation (SW) along the trajectories that arrive at any given location between 10:00 and 14:00 LT (SI Appendix, Figure S11B). We found that beyond the *boom* region, the accumulated SW no longer increased. This is because trajectories reaching further downwind started earlier and traveled longer during the nighttime. Lastly, the maximum O_3 mixing ratio location is not always the same during the whole simulation period because of variations in the plume trajectory. Looking at individual days (SI Appendix, Figure S5), the maximum O_3 can be higher (up to 60 ppbv) and can be further away (up to 150 km) than we have described for the average day. Thus, the location of the *boom* region is also determined by the variability of the plume position. SI Appendix, Figure S11A shows the density of air mass trajectories, which decrease significantly beyond the western border of the *boom* region, defusing the maximum O_3 found there.

Summarizing, our simulations show that the high amounts of O_3 present in the *boom* region, beginning at 10:00 (LT), are the result of local production and not due to O_3 transport from other areas. The elevated O_3 concentrations (10:00−14:00 LT) are due to the mix of night-time and early morning transport of NO*x* and HCHO from Manaus and BVOCs emitted from the forest during the day. The combination of sufficient solar radiation and the mixing of these O_3 precursors create conditions ideal for O_3 production in the *boom* region, far from Manaus, with a maximum mixing ratio at 14:00 LT. The location of the *boom* region depends on the plume age (primarily through the total solar irradiation) and the wind velocity. This shows that nocturnally reserved compounds transported over long distances such as NO*x* in this study, or isoprene as reported by Millet et al.,[43] can have a powerful effect on O_3 and SOA, leading to the large-scale local production of these chemicals in areas far from the source of their precursors.

Manaus Plume Impact on SOA Formation in the Central Amazon Region. Our simulations show that Manaus emissions significantly impact SOA, defined as the sum of biogenic (BSOA) and anthropogenic (ASOA) secondary organic aerosols. We find that SOA is maximum ∼140 km downwind of Manaus around 14 h LT (Figure 4A, B), the same region of the maximum O_3 concentration. Values reach 1.0 to 1.8 μgm^{-3}, well above background levels. These high concentrations reach a larger area (SI Appendix, Figure S4) than previously estimated.[5,14−16] However, Palm et al.[18] estimated that some amount (0−12 μgm^{-3}) of SOA could form beyond T3 using an oxidation flow reactor at the site.

Figure 4C, D shows the strong correspondence between atmospheric oxidants O*x*, here characterized by the sum of O_3 and NO_2,[44,45] and the SOA concentration. The remarkable correlation between O*x* and SOA during daytime (SI Appendix, Figure S12) is explained by the fact that both of them rely on the photochemical production of radicals and VOC oxidation. These results show that the *boom* region presents a powerful oxidative condition, driven mostly by the OH concentration (SI Appendix, Figure S14) and an increase in O_3 (Figure 2B, D), which is a result of combining urban emissions, sufficient solar radiation, and high BVOC concentrations, as previously discussed. To understand what controls the peak of the SOA concentration in the *boom* region, we look at BSOA and ASOA separately (SI Appendix, Figure S13). The concentration of ASOA in the pollution plume is very close to the background values near Manaus. It increases up to 140 km downwind of Manaus, reaching 0.5 to 0.8 μgm^{-3}, and decreases to background values again around 250−300 km downwind. The production of ASOA depends on the oxidation of aromatic volatile organic compounds (AVOCs), which are only emitted in the urban environment, and they are not readily oxidized in the presence of O_3.[18] AVOCs and NO*x* are both consumed for the production of SOA and O_3, and hence, their mixing ratios only decrease as the plume disperses. Therefore, the ASOA concentration is maximum at a certain distance (140 km) downwind of Manaus, in agreement with the amount of the oxidant hydroxyl radical (OH) available (SI Appendix, Figure S14).

The situation is different for the biogenic contribution. The concentration of BSOA is already higher over Manaus than the background value, with values of 0.2 to 0.5 μgm^{-3}. The BSOA concentration increases up to 140 km downwind of Manaus, reaching 0.6 to 1.0 μgm^{-3} and stabilizing further downwind. The production of BSOA depends on the oxidation of BVOCs, nonaromatic compounds emitted in abundance by the forest,[18,38,46] which can be oxidized in the presence of O_3. Because BVOCs are consumed and emitted as the plume travels over the forest, BSOA mixing ratios do not fall so sharply (SI Appendix, Figure S15A). Indeed, the BSOA mixing ratios start to increase beyond 140 km downwind of Manaus city, reaching background values around 250 km downwind of Manaus. Moreover, because O*x* stays high, the production of BSOA continues beyond the *boom* region. The oxidative capacity of the Amazonian atmosphere is broadly determined by the presence of OH and O_3. Our simulations show that the urban emissions modify this capacity significantly. In terms of SOA production, the Manaus plume contributes more by the extra production of BSOA than by the production of ASOA. Indeed, the maximum contribution of ASOA is ∼50% around 140 km downwind of Manaus, dropping to ∼15% around 250 km downwind of Manaus. Of course, the dynamical processes discussed in the previous section are also relevant here.

The plume reaching the *boom* region between 10-14 h LT left Manaus early in the morning. Anthropogenic oxidants transported aloft are mixed with BVOCs at the surface after the NBL is eroded, circa 8−9 h LT.[39] The position of the SOA plume varies from day to day, and so does the region of maximum SOA concentration, which can reach beyond 200 km downwind of Manaus (SI Appendix, Figure S16). OA measurements at the T3 site (SI Appendix, Figure S17), as well as from aircraft (SI Appendix, Figure S21), were compared with simulated SOA to evaluate the model's SOA production downwind Manaus. Our results give further evidence of SOA production in the perturbed forest environment and show the mechanism, intensity, and reach of this perturbation.

This research shows the significant impact urban center emissions can have on SOA and O_3 production in the tropical environment. With anthropogenic emissions from Manaus, the O_3 and SOA production peaks ∼150−200 km downwind of Manaus city, much further downwind than any monitoring station, and beyond the T3 site (the furthest downwind site) of the GoAmazon2014/5 campaign. With favorable meteorological conditions, emissions of NO*x* from Manaus can reach regions ∼70−200 km downwind,[14,15,32] giving them the opportunity to mix with biogenic VOCs from the forest and leading to conditions favorable to O_3 formation. NO*x* concentrations downwind of Manaus begin to fall to background levels (<1ppbv) only beyond ∼300 km downwind of Manaus. This large area with elevated NO*x* values has very significant impacts on SOA and O_3 production, with O_3 ∼40 ppbv and SOA ∼1.8 $\mu g\ m^{-3}$, above the background. The production of O_3 downwind of Manaus is also significant as it is an important oxidant gas for BSOA formation and can impact forest health. The simulations provide unique insights in understanding how the O_3 and SOA formation mechanisms in a relatively pristine tropical region may be affected by anthropogenic contributions ∼150−200 km away from an urban center.

O_3 in the perturbed Amazon forest is predominantly produced by the mixing of and interactions between urban pollutants and biogenic VOCs.[9,32] Therefore, the O_3 enhancement depends on the distance from the urban emissions, with varying behavior at ranges farther than 200 km downwind of Manaus (Figure 2). The contribution of NO*x* from Manaus is one of the key elements impacting O_3 production in regions affected by the Manaus pollution plume. The results show that the Manaus NO*x* emissions and day-time emitted BVOCs from the forest, when combined with sufficient solar radiation, create conditions ideal for O_3 enhancement in the *boom* region, the region of the highest O_3 mixing ratios at 14:00 (LT) (Figure 2F). At the heart of our study is a WRF-chem simulation of the area around Manaus. This simulation was validated with data from ground-based, aircraft, and remote-sensing sources. The simulations accurately represent the meteorological fields, photochemistry, and transport of aerosols, O_3, and CO. Agreement between simulated and observed mixing ratios for a number of chemical species related to the production and transport of SOA and O_3 was found.

It is difficult to determine if SOA mass is anthropogenic or biogenic in origin or a combination of both, given only aircraft experimental data.[14] However, a modeling study that represents the SOA well, as ours does, gives this partition.

https://doi.org/10.1021/acs.est.2c01358
Environ. Sci. Technol. 2022, 56, 9924−9935

Future work could be done using this and similar simulations to find relationships between the partition ratio and other atmospheric variables measured by aircraft in the Amazon region. The emissions of urban centers such as Manaus have a significant impact on the chemistry in their surroundings, creating a more oxidative atmosphere even far downwind of the urban area. One of the biggest consequences of high anthropogenic emissions is their effect on human health and vegetation. The increase in O_3 production, especially in regions far from Manaus in otherwise pristine forest, may affect the forest photosynthesis ratio and primary productivity, meaning that studies like this are critical for the development of O_3 pollution control strategies in tropical forest regions.

Large SOA and O_3 production may be occurring in other similar regions where urban centers are located within tropical forests, such as Africa, Indonesia, and other Amazonian regions with urban centers. The cities of Santarém and Belém, also surrounded by Amazonian forest, may have similar impacts on SOA and O_3 production and represent potential regions to be investigated. The high O3 levels during the day may have a significant and damaging effect on vegetation in the central Amazon. Tropical forests evolved with O_3 values even lower than ones found in boreal and temperate forests (> ∼40 ppbv).[47,48] Thus, the threshold of O_3 needed to cause damage to vegetation is also likely lower. O_3 may begin to have potential impacts on vegetation above ∼20−30 ppbv.[49] However, most botanic assessments do not account for the biodiversity of the Amazon forest, further hampering our ability to estimate the extent of the O_3 damage.

In summary, our findings indicate that anthropogenic activities, namely, the pollution emissions of urban centers, have a unique and significant effect on tropical forest regions far from their source. Because the mixing of anthropogenic and biogenic chemical species is a common phenomenon, because of favorable meteorological conditions, large amounts of NO*x* emitted in Manaus reach regions 150−200 km downwind of the urban area. This, combined with high solar radiation and VOCs emitted in Manaus and by the forest, creates a perfect scenario for O_3 production, which consequently contributes to SOA production, as the O_3 is a direct oxidant to BSOA production.[18] This leads to high O_3 and SOA concentrations of greater than ∼47 ppbv and 1.8 $\mu g\ m^{-3}$, respectively, 150−200 km downwind of Manaus. These highly oxidative areas are under a NO*x*-limited regime so that changes in NO*x* emissions from Manaus have a large impact on O_3 and SOA production. Future work should be done to confirm these results with in situ measurements by drone or aircraft. The results found in this research will be checked by and used to guide new field campaigns, such as the Chemistry of the Atmosphere-Field Experiment in Brazil (CAFE-Brazil) and the Fluvial Observations of key climatic drivers in The Amazon (FLOAT-Amazon). These projects are scheduled to begin in 2022.

■ ASSOCIATED CONTENT

Supporting Information

The Supporting Information is available free of charge at https://pubs.acs.org/doi/10.1021/acs.est.2c01358.

> Additional details on the WRF-Chem numerical experiments such as configurations, statistical performance, and additional comparisons with ground and aircraft measurements data; information on the geographical positions of the sampling stations and analyses of the effect of the Manaus plume on the *boom* region for other simulated days; additional HYSPLIT analyses to understand the origin of different air masses contributing to the maximum O_3 mixing ratio in order to compute the density of polluted air masses for different locations surrounding Manaus; and other supplementary figures (PDF)

■ AUTHOR INFORMATION

Corresponding Authors

Janaina P. Nascimento − *National Institute for Amazonian Research, Manaus, AM 69.060-000, Brazil; Amazonas State University, Manaus, AM 69470000, Brazil; NOAA Global Systems Laboratory, Boulder, Colorado 80305, United States;* orcid.org/0000-0002-1904-3751; Email: janaina.nascimento@noaa.gov

Megan M. Bela − *NOAA Chemical Sciences Laboratory, Boulder, Colorado 80305, United States;* orcid.org/0000-0002-3998-9990; Email: megan.bela@noaa.gov

Authors

Henrique M. J. Barbosa − *Institute of Physics, University of Sao Paulo, Sao Paulo, SP 05508-090, Brazil*

Alessandro L. Banducci − *Department of Physics, Colorado State University, Fort Collins, Colorado 80523, United States*

Luciana V. Rizzo − *Department of Environmental Sciences, Institute of Environmental, Chemical and Pharmaceutical Sciences, Federal University of Sao Paulo, Sao Paulo, SP 09913-030, Brazil*

Angel Liduvino Vara-Vela − *Department of Atmospheric Sciences, Institute of Astronomy, Geophysics and Atmospheric Sciences, University of Sao Paulo, Sao Paulo 05508-090, Brazil; Federal University of Technology, Londrina, Puerto Rico 86047-125, Brazil;* orcid.org/0000-0002-4972-4486

Bruno B. Meller − *Institute of Physics, University of Sao Paulo, Sao Paulo, SP 05508-090, Brazil*

Helber Gomes − *Institute of Atmospheric Sciences, Federal University of Alagoas, Maceio, Alabama 57072-900, Brazil; Department of Meteorology, Federal University of Campina Grande, Campina Grande, PB 58428-830, Brazil*

André Cezar − *Institute of Physics, University of Sao Paulo, Sao Paulo, SP 05508-090, Brazil*

Marco A. Franco − *Institute of Physics, University of Sao Paulo, Sao Paulo, SP 05508-090, Brazil;* orcid.org/0000-0002-2279-7722

Milena Ponczek − *Institute of Physics, University of Sao Paulo, Sao Paulo, SP 05508-090, Brazil*

Stefan Wolff − *Multiphase Chemistry Department, Max Planck Institute for Chemistry, Mainz 55128, Germany*

Paulo Artaxo − *Institute of Physics, University of Sao Paulo, Sao Paulo, SP 05508-090, Brazil*

Complete contact information is available at: https://pubs.acs.org/10.1021/acs.est.2c01358

Notes

The authors declare no competing financial interest.

The GoAmazon2014/5 experiment data are available from the ARM website: https://www.arm.gov/research/campaigns/amf2014goamazon and from the Laboratory of Atmospheric Physics−LFA website: http://ftp.lfa.if.usp.br/ftp/public/LFA_Processed_Data/. Aircraft measurements from the GoAma-

https://doi.org/10.1021/acs.est.2c01358
Environ. Sci. Technol. 2022, 56, 9924−9935

zon2014/5 field campaign used in this study are publicly available on the Atmospheric Radiation Measurement (ARM) website: http://campaign.arm.gov/goamazon2014/observations/. The simulations and analysis code generated for this study are available upon request from JPN.

■ ACKNOWLEDGMENTS

We acknowledge support from the central office of the Large-Scale Biosphere−Atmosphere Experiment in Amazonia (LBA), coordinated by the National Institute of Amazonian Research (INPA) and the Amazonas State University (UEA), Amazonas, Brazil. J.P.N. thanks the Brazilian Federal Agency for Support and Evaluation of Graduate Education (CAPES) for a graduate fellowship (grant no. 88882.444345/2018-01), linked to the doctoral program in Climate and Environment (CLIAMB), and for supporting seven months of a visiting graduate student program at the NOAA Earth System Research Laboratory (grant no. 88881.190103/2018-01). J.P.N. also thanks CIRES and NOAA ESRL for financial and logistical support. We thank Michael Trainer for providing support and knowledge during the research. We thank Manish Shrivastava for providing the WRF-Chem simulation output for comparison with this work. We thank Gilberto Fish for providing the planetary boundary layer observed data. We thank Steven Jefferts, Stefania Romisch, and Samuel Brewer for facilitating communication between members of this collaboration. We are grateful to Bruno Takeshi, Luiz Candido, Renata Teixeira, and Delano Campos, for instrument operation and data analysis. Finally, we thank Richard Tisinai, for IT support. Marco A. Franco acknowledges a scholarship from CNPq (grant no. 169842/2017-7), for supporting his doctoral studies at the IFUSP, Sao Paulo, Brazil, and CAPES (grant no. 88887.368025/2019-00), for supporting six months of a visiting graduate student program at the Max Planck Institute for Chemistry, Mainz, Germany. Bruno Backes Meller acknowledges a scholarship from CNPq (grant no. 133393/2019-4) for supporting his Masters at the IFUSP, Sao Paulo, Brazil. Helber Gomes acknowledges funding from CAPES (grant no. 757/2017). Paulo Artaxo acknowledges funding from FAPESP (grant no. 2017/17047-0). This work was supported in part by the NOAA Cooperative Agreement with CIRES, NA17OAR4320101. Additional funding was provided by the Sao Paulo State Research Foundation (grant no. FAPESP 2013/05014-0, FAPESP 2013/50510-5, FAPESP 2013/10156-8, and FAPESP 2017/17047-0).

■ REFERENCES

(1) Andreae, M. O.; Acevedo, O. C.; Araùjo, A.; Artaxo, P.; Barbosa, C. G. G.; Barbosa, H. M. J.; Brito, J.; Carbone, S.; Chi, X.; Cintra, B. B. L.; da Silva, N. F.; Dias, N. L.; Dias-Junior, C. Q.; Ditas, F.; Ditz, R.; Godoi, A. F. L.; Godoi, R. H. M.; Heimann, M.; Hoffmann, T.; Kesselmeier, J.; Könemann, T.; Krüger, M. L.; Lavric, J. V.; Manzi, A. O.; Lopes, A. P.; Martins, D. L.; Mikhailov, E. F.; Moran-Zuloaga, D.; Nelson, B. W.; Nölscher, A. C.; Santos Nogueira, D.; Piedade, M. T. F.; Pöhlker, C.; Pöschl, U.; Quesada, C. A.; Rizzo, L. V.; Ro, C.-U.; Ruckteschler, N.; Sá, L. D. A.; de Oliveira Sá, M.; Sales, C. B.; dos Santos, R. M. N.; Saturno, J.; Schöngart, J.; Sörgel, M.; de Souza, C. M.; de Souza, R. A. F.; Su, H.; Targhetta, N.; Tóta, J.; Trebs, I.; Trumbore, S.; van Eijck, A.; Walter, D.; Wang, Z.; Weber, B.; Williams, J.; Winderlich, J.; Wittmann, F.; Wolff, S.; Yáñez-Serrano, A. M. The Amazon Tall Tower Observatory (ATTO): overview of pilot measurements on ecosystem ecology, meteorology, trace gases, and aerosols. *Atmos. Chem. Phys.* **2015**, *15*, 10723−10776.

(2) Yáñez-Serrano, A. M.; Bourtsoukidis, E.; Alves, E. G.; Bauwens, M.; Stavrakou, T.; Llusià, J.; Filella, I.; Guenther, A.; Williams, J.; Artaxo, P.; Sindelarova, K.; Doubalova, J.; Kesselmeier, J.; Peñuelas, J. Amazonian biogenic volatile organic compounds under global change. *Global Change Biol.* **2020**, *26*, 4722−4751.

(3) Greenberg, J. P.; Zimmerman, P. R. Nonmethane hydrocarbons in remote tropical, continental, and marine atmospheres. *J. Geophys. Res.* **1984**, *89*, 4767.

(4) Kesselmeier, J.; Kuhn, U.; Rottenberger, S.; Biesenthal, T.; Wolf, A.; Schebeske, G.; Andreae, M. O.; Ciccioli, P.; Brancaleoni, E.; Frattoni, M.; Oliva, S. T.; Botelho, M. L.; Silva, C. M. A.; Tavares, T. M. Concentrations and species composition of atmospheric volatile organic compounds (VOCs) as observed during the wet and dry season in Rondônia (Amazonia). *J. Geophys. Res.* **2002**, *107*, 8053.

(5) de Sá, S. S.; Palm, B. B.; Campuzano-Jost, P.; Day, D. A.; Hu, W.; Isaacman-VanWertz, G.; Yee, L. D.; Brito, J.; Carbone, S.; Ribeiro, I. O.; Cirino, G. G.; Liu, Y.; Thalman, R.; Sedlacek, A.; Funk, A.; Schumacher, C.; Shilling, J. E.; Schneider, J.; Artaxo, P.; Goldstein, A. H.; Souza, R. A. F.; Wang, J.; McKinney, K. A.; Barbosa, H.; Alexander, M. L.; Jimenez, J. L.; Martin, S. T. Urban influence on the concentration and composition of submicron particulate matter in central Amazonia. *Atmos. Chem. Phys.* **2018**, *18*, 12185−12206.

(6) de Sá, S. S.; Rizzo, L. V.; Palm, B. B.; Campuzano-Jost, P.; Day, D. A.; Yee, L. D.; Wernis, R.; Isaacman-VanWertz, G.; Brito, J.; Carbone, S.; Liu, Y. J.; Sedlacek, A.; Springston, S.; Goldstein, A. H.; Barbosa, H. M. J.; Alexander, M. L.; Artaxo, P.; Jimenez, J. L.; Martin, S. T. Contributions of biomass-burning, urban, and biogenic emissions to the concentrations and light-absorbing properties of particulate matter in central Amazonia during the dry season. *Atmos. Chem. Phys.* **2019**, *19*, 7973−8001.

(7) Teixeira, P. R.; Freitas, S. R.; Correia, F. W.; Manzi, A. O. Moveim v1.0: Development of a bottom up motor vehicular emission inventories for the urban area of Manaus in central amazon rainforest. *Geosci. Model. Dev. Discuss.* **2018**, 1−21.

(8) Abou Rafee, S. A.; Martins, L. D.; Kawashima, A. B.; Almeida, D. S.; Morais, M. V. B.; Souza, R. V. A.; Oliveira, M. B. L.; Souza, R. A. F.; Medeiros, A. S. S.; Urbina, V.; Freitas, E. D.; Martin, S. T.; Martins, J. A. Contributions of mobile, stationary and biogenic sources to air pollution in the Amazon rainforest: a numerical study with the WRF-Chem model. *Atmos. Chem. Phys.* **2017**, *17*, 7977−7995.

(9) Kuhn, U.; Ganzeveld, L.; Thielmann, A.; Dindorf, T.; Schebeske, G.; Welling, M.; Sciare, J.; Roberts, G.; Meixner, F. X.; Kesselmeier, J.; Lelieveld, J.; Kolle, O.; Ciccioli, P.; Lloyd, J.; Trentmann, J.; Artaxo, P.; Andreae, M. O. Impact of Manaus City on the Amazon Green Ocean atmosphere: ozone production, precursor sensitivity and aerosol load. *Atmos. Chem. Phys.* **2010**, *10*, 9251−9282.

(10) Martin, S. T.; Artaxo, P.; Machado, L. A. T.; Manzi, A. O.; Souza, R. A. F.; Schumacher, C.; Wang, J.; Andreae, M. O.; Barbosa, H. M. J.; Fan, J.; Fisch, G.; Goldstein, A. H.; Guenther, A.; Jimenez, J. L.; Pöschl, U.; Silva Dias, M. A.; Smith, J. N.; Wendisch, M. Introduction: Observations and Modeling of the Green Ocean Amazon (GoAmazon2014/5). *Atmos. Chem. Phys.* **2016**, *16*, 4785−4797.

(11) Geng, F.; Zhao, C.; Tang, X.; Lu, G.; Tie, X. Analysis of ozone and vocs measured in shanghai: A case study. *Atmos. Environ.* **2007**, *41*, 989−1001.

(12) Sillman, S. The use of NOy, H_2O_2, and HNO_3 as indicators for ozone-no x-hydrocarbon sensitivity in urban locations. *J. Geophys. Res.: Atmos.* **1995**, *100*, 14175−14188.

(13) Medeiros, A. S. S.; Calderaro, G.; Guimarães, P. C.; Magalhaes, M. R.; Morais, M. V. B.; Rafee, S. A. A.; Ribeiro, I. O.; Andreoli, R. V.; Martins, J. A.; Martins, L. D.; Martin, S. T.; Souza, R. A. F. Power plant fuel switching and air quality in a tropical, forested environment. *Atmos. Chem. Phys.* **2017**, *17*, 8987−8998.

(14) Shilling, J. E.; Pekour, M. S.; Fortner, E. C.; Artaxo, P.; de Sá, S.; Hubbe, J. M.; Longo, K. M.; Machado, L. A. T.; Martin, S. T.; Springston, S. R.; Tomlinson, J.; Wang, J. Aircraft observations of the chemical composition and aging of aerosol in the Manaus urban

plume during GoAmazon 2014/5. *Atmos. Chem. Phys.* **2018**, *18*, 10773−10797.

(15) Shrivastava, M.; Andreae, M. O.; Artaxo, P.; Barbosa, H. M. J.; Berg, L. K.; Brito, J.; Ching, J.; Easter, R. C.; Fan, J. W.; Fast, J. D.; Feng, Z.; Fuentes, J. D.; Glasius, M.; Goldstein, A. H.; Alves, E. G.; Gomes, H.; Gu, D.; Guenther, A.; Jathar, S. H.; Kim, S.; Liu, Y.; Lou, S. J.; Martin, S. T.; McNeill, V. F.; Medeiros, A.; de Sa, S. S.; Shilling, J. E.; Springston, S. R.; Souza, R. A. F.; Thornton, J. A.; Isaacman-VanWertz, G.; Yee, L. D.; Ynoue, R.; Zaveri, R. A.; Zelenyuk, A.; Zhao, C. Urban pollution greatly enhances formation of natural aerosols over the Amazon rainforest. *Nat. Commun.* **2019**, *10*, 1046.

(16) Nascimento, J. P.; Bela, M. M.; Meller, B. B.; Banducci, A. L.; Rizzo, L. V.; Vara-Vela, A. L.; Barbosa, H. M. J.; Gomes, H.; Rafee, S. A. A.; Franco, M. A.; Carbone, S.; Cirino, G. G.; Souza, R. A. F.; McKeen, S. A.; Artaxo, P. Aerosols from anthropogenic and biogenic sources and their interactions − modeling aerosol formation, optical properties, and impacts over the central Amazon basin. *Atmos. Chem. Phys.* **2021**, *21*, 6755−6779.

(17) Cirino, G.; Brito, J.; Barbosa, H. M. J.; Rizzo, L. V.; Tunved, P.; de Sá, S. S.; Jimenez, J. L.; Palm, B. B.; Carbone, S.; Lavric, J.; Souza, R. A. F.; Wolff, S.; Walter, D.; Tota, J.; Oliveira, M. B. L.; Martin, S. T.; Artaxo, P. Observations of Manaus urban plume evolution and interaction with biogenic emissions in GoAmazon 2014/5. *Atmos. Environ.* **2018**, *191*, 513−524.

(18) Palm, B. B.; de Sá, S. S.; Day, D. A.; Campuzano-Jost, P.; Hu, W.; Seco, R.; Sjostedt, S. J.; Park, J.-H.; Guenther, A. B.; Kim, S.; Brito, J.; Wurm, F.; Artaxo, P.; Thalman, R.; Wang, J.; Yee, L. D.; Wernis, R.; Isaacman-VanWertz, G.; Goldstein, A. H.; Liu, Y.; Springston, S. R.; Souza, R.; Newburn, M. K.; Alexander, M. L.; Martin, S. T.; Jimenez, J. L. Secondary organic aerosol formation from ambient air in an oxidation flow reactor in central Amazonia. *Atmos. Chem. Phys.* **2018**, *18*, 467−493.

(19) Rap, A.; Spracklen, D. V.; Mercado, L.; Reddington, C. L.; Haywood, J. M.; Ellis, R. J.; Phillips, O. L.; Artaxo, P.; Bonal, D.; Restrepo Coupe, N.; Butt, N. Fires increase Amazon forest productivity through increases in diffuse radiation. *Geophys. Res. Lett.* **2015**, *42*, 4654−4662.

(20) Pacifico, F.; Folberth, G. A.; Sitch, S.; Haywood, J. M.; Rizzo, L. V.; Malavelle, F. F.; Artaxo, P. Biomass burning related ozone damage on vegetation over the Amazon forest: a model sensitivity study. *Atmos. Chem. Phys.* **2015**, *15*, 2791−2804.

(21) Lim, H. J.; Carlton, A. G.; Turpin, B. J. Isoprene forms secondary organic aerosol through cloud processing: Model simulations. *Environ. Sci. Technol.* **2005**, *39*, 4441−4446.

(22) Forkel, R.; Werhahn, J.; Hansen, A. B.; McKeen, S.; Peckham, S.; Grell, G.; Suppan, P. Effect of aerosol radiation feedback on regional air quality − A case study with WRF/Chem. *Atmos. Environ.* **2012**, *53*, 202−211.

(23) Tuccella, P.; Curci, G.; Grell, G. A.; Visconti, G.; Crumeyrolle, S.; Schwarzenboeck, A.; Mensah, A. A. A new chemistry option in WRF-Chem v. 3.4 for the simulation of direct and indirect aerosol effects using VBS: evaluation against IMPACT-EUCAARI data. *Geosci. Model Dev.* **2015**, *8*, 2749−2776.

(24) Thalman, R.; de Sá, S. S.; Palm, B. B.; Barbosa, H. M. J.; Pöhlker, M. L.; Alexander, M. L.; Brito, J.; Carbone, S.; Castillo, P.; Day, D. A.; Kuang, C.; Manzi, A.; Ng, N. L.; Sedlacek, A. J., III; Souza, R.; Springston, S.; Watson, T.; Pöhlker, C.; Pöschl, U.; Andreae, M. O.; Artaxo, P.; Jimenez, J. L.; Martin, S. T.; Wang, J. CCN activity and organic hygroscopicity of aerosols downwind of an urban region in central Amazonia: seasonal and diel variations and impact of anthropogenic emissions. *Atmos. Chem. Phys.* **2017**, *17*, 11779−11801.

(25) Zhao, B.; Fast, J. D.; Donahue, N. M.; Shrivastava, M.; Schervish, M.; Shilling, J. E.; Gordon, H.; Wang, J.; Gao, Y.; Zaveri, R. A.; Liu, Y.; Gaudet, B. Impact of Urban Pollution on Organic-Mediated New-Particle Formation and Particle Number Concentration in the Amazon Rainforest. *Environ. Sci. Technol.* **2021**, *55*, 4357−4367.

(26) Rosenfeld, D.; Lohmann, U.; Raga, G. B.; O'Dowd, C. D.; Kulmala, M.; Fuzzi, S.; Reissell, A.; Andreae, M. O. Flood or drought: How do aerosols affect precipitation? *Science* **2008**, *321*, 1309−1313.

(27) Fan, J.; Rosenfeld, D.; Zhang, Y.; Giangrande, S. E.; Li, Z.; Machado, L. A.; Martin, S. T.; Yang, Y.; Wang, J.; Artaxo, P.; Barbosa, H. M.; Braga, R. C.; Comstock, J. M.; Feng, Z.; Gao, W.; Gomes, H. B.; Mei, F.; Pöhlker, C.; Pöhlker, M. L.; Pöschl, U.; de Souza, R. A. F. Substantial convection and precipitation enhancements by ultrafine aerosol particles. *Science* **2018**, *359*, 411−418.

(28) Ou, J.; Huang, Z.; Klimont, Z.; Jia, G.; Zhang, S.; Li, C.; Meng, J.; Mi, Z.; Zheng, H.; Shan, Y.; Louie, P. K. K.; Zheng, J.; Guan, D. Role of export industries on ozone pollution and its precursors in China. *Nat. Commun.* **2020**, *11*, 5492.

(29) Geng, F.; Tie, X.; Guenther, A.; Li, G.; Cao, J.; Harley, P. Effect of isoprene emissions from major forests on ozone formation in the city of Shanghai, China. *Atmos. Chem. Phys.* **2011**, *11*, 10449−10459.

(30) Nogueira, T.; Dominutti, P. A.; De Carvalho, L. R. F.; Fornaro, A.; Andrade, M. F. Formaldehyde and acetaldehyde measurements in urban atmosphere impacted by the use of ethanol biofuel: Metropolitan Area of Sao Paulo, 2012−2013. *Fuel* **2014**, *134*, 505−513.

(31) Carter, W. P. L. *Updated maximum incremental reactivity scale and hydrocarbon bin reactivities for regulatory application*; College of Engineering Center for Environmental Research and Technology-University of California, 2010. Riverside: <http://www.arb.ca.gov/research/reactivity/mir09.pdf>.

(32) Martin, S. T.; Artaxo, P.; Machado, L.; Manzi, A. O.; Souza, R.; Schumacher, C.; Wang, J.; Biscaro, T.; Brito, J.; Calheiros, A.; Jardine, K.; Medeiros, A.; Portela, B.; de Sá, S. S.; Adachi, K.; Aiken, A. C.; Albrecht, R.; Alexander, L.; Andreae, M. O.; Barbosa, H. M. J.; Buseck, P.; Chand, D.; Comstock, J. M.; Day, D. A.; Dubey, M.; Fan, J.; Fast, J.; Fisch, G.; Fortner, E.; Giangrande, S.; Gilles, M.; Goldstein, A. H.; Guenther, A.; Hubbe, J.; Jensen, M.; Jimenez, J. L.; Keutsch, F. N.; Kim, S.; Kuang, C.; Laskin, A.; McKinney, K.; Mei, F.; Miller, M.; Nascimento, R.; Pauliquevis, T.; Pekour, M.; Peres, J.; Petäjä, T.; Pöhlker, C.; Pöschl, U.; Rizzo, L.; Schmid, B.; Shilling, J. E.; Dias, M. A. S.; Smith, J. N.; Tomlinson, J. M.; Tóta, J.; Wendisch, M. The Green Ocean Amazon experiment (GoAmazon2014/5) observes pollution affecting gases, aerosols, clouds, and rainfall over the rain forest. *Bull. Am. Meteorol. Soc.* **2017**, *98*, 981−997.

(33) Lin, M.; Horowitz, L. W.; Xie, Y.; Paulot, F.; Malyshev, S.; Shevliakova, E.; Finco, A.; Gerosa, G.; Kubistin, D.; Pilegaard, K. Vegetation feedbacks during drought exacerbate ozone air pollution extremes in Europe. *Nat. Clim. Change* **2020**, *10*, 444−451.

(34) Artaxo, P.; Rizzo, L. V.; Brito, J. F.; Barbosa, H. M.; Arana, A.; Sena, E. T.; Cirino, G. G.; Bastos, W.; Martin, S. T.; Andreae, M. O. Atmospheric aerosols in Amazonia and land use change: from natural biogenic to biomass burning conditions. *Faraday Discuss.* **2013**, *165*, 203−235.

(35) Bela, M. M.; Longo, K. M.; Freitas, S. R.; Moreira, D. S.; Beck, V.; Wofsy, S. C.; Gerbig, C.; Wiedemann, K.; Andreae, M. O.; Artaxo, P. Ozone production and transport over the Amazon Basin during the dry-to-wet and wet-to-dry transition seasons. *Atmos. Chem. Phys.* **2015**, *15*, 757−782.

(36) Gu, D.; Guenther, A. B.; Shilling, J. E.; Yu, H.; Huang, M.; Zhao, C.; Yang, Q.; Martin, S. T.; Artaxo, P.; Kim, S.; Seco, R.; Stavrakou, T.; Longo, K. M.; Tóta, J.; de Souza, R. A. F.; Vega, O.; Liu, Y.; Shrivastava, M.; Alves, E. G.; Santos, F. C.; Leng, G.; Hu, Z. Airborne observations reveal elevational gradient in tropical forest isoprene emissions. *Nat. Commun.* **2017**, *8*, 15541.

(37) Alves, E. G.; Tóta, J.; Turnipseed, A.; Guenther, A. B.; Vega Bustillos, J. O. W.; Santana, R. A.; Cirino, G. G.; Tavares, J. V.; Lopes, A. P.; Nelson, B. W.; de Souza, R. A.; Gu, D.; Stavrakou, T.; Adams, D. K.; Wu, J.; Saleska, S.; Manzi, A. O. Leaf phenology as one important driver of seasonal changes in isoprene emissions in central Amazonia. *Biogeosciences* **2018**, *15*, 4019−4032.

(38) Guenther, A. B.; Jiang, X.; Heald, C. L.; Sakulyanontvittaya, T.; Duhl, T.; Emmons, L. K.; Wang, X. The Model of Emissions of Gases and Aerosols from Nature version 2.1 (MEGAN2.1): an extended and

updated framework for modeling biogenic emissions. *Geosci. Model Dev.* **2012**, *5*, 1471−1492.
(39) Carneiro, R. G.; Fisch, G. Observational analysis of the daily cycle of the planetary boundary layer in the central Amazon during a non-El Niño year and El Ni o year (GoAmazon project 2014/5). *Atmos. Chem. Phys.* **2020**, *20*, 5547−5558.
(40) Palmer, P. I.; Marvin, M. R.; Siddans, R.; Kerridge, B. J.; Moore, D. P. Nocturnal survival of isoprene linked to formation of upper tropospheric organic aerosol. *Science* **2022**, *375*, 562−566.
(41) Brown, S. S.; Stutz, J. Nighttime Radical Observations and Chemistry. *Chem. Soc. Rev.* **2012**, *41*, 6405−6447.
(42) Mentel, T. F.; Bleilebens, D.; Wahner, A. A study of nighttime nitrogen oxide oxidation in a large reaction chamber − the fate of NO_2, N_2O_5, HNO_3 and O_3 at different humidities. *Atmos. Environ.* **1996**, *30*, 4007−4020.
(43) Millet, D. B.; Baasandorj, M.; Hu, L.; Mitroo, D.; Turner, J.; Williams, B. J. Nighttime Chemistry and Morning Isoprene Can Drive Urban Ozone Downwind of a Major Deciduous Forest. *Environ. Sci. Technol.* **2016**, *50*, 4335−4342.
(44) Clapp, L. J.; Jenkin, M. E. Analysis of the relationship between ambient levels of O3, NO2 and NO as a function of NO*x* in the UK. *Atmos. Environ.* **2001**, *35*, 6391−6405.
(45) Kley, D.; Geiss, H.; Mohnen, V. A. Tropospheric ozone at elevated sites and precursor emissions in the United-States and Europe. *Atmos. Environ.* **1994**, *28*, 149−158.
(46) Ahmadov, R.; McKeen, S.; Robinson, A.; Bahreini, R.; Middlebrook, A.; De Gouw, J.; Meagher, J.; Hsie, E.-Y.; Edgerton, E.; Shaw, S.; Trainer, M. A volatility basis set model for summertime secondary organic aerosols over the eastern United States in 2006. *J. Geophys. Res.* **2012**, *117*, D06301.
(47) Ashmore, M. Assessing the Future Global Impacts of Ozone on Vegetation. *Plant Cell Environ.* **2005**, *28*, 949−964.
(48) Felzer, B.; Cronin, T.; Reilly, J. M.; Wang, X. Impact of ozone on trees and crops. *C. R. Geosci.* **2007**, *339*, 784−798.
(49) Anav, A.; De Marco, A.; Proietti, C.; Alessandri, A.; Dell'Aquila, A.; Cionni, I.; Friedlingstein, P.; Khvorostyanov, D.; Menut, L.; Paoletti, E.; Sicard, P.; Sitch, S.; Vitale, M. Comparing concentration-based (AOT40) and stomatal uptake (PODY) metrics for ozone risk assessment to European forests. *Global Change Biol.* **2016**, *22*, 1608−1627.
(50) Grell, G. A.; Peckham, S. E.; Schmitz, R.; McKeen, S.; Frost, G.; Skamarock, W. C.; Eder, B. Fully coupled "online" chemistry within the WRF model. *Atmos. Environ.* **2005**, *39*, 6957−6975.
(51) Fast, J. D.; Gustafson, W. I.; Easter, R. C.; Zaveri, R. A.; Barnard, J. C.; Chapman, E. G.; Grell, G. A.; Peckham, S. E. Evolution of ozone, particulates, and aerosol direct radiative forcing in the vicinity of Houston using a fully coupled meteorology-chemistry-aerosol model. *J. Geophys. Res.: Atmos.* **2006**, *111*, D21305.
(52) Vara-Vela, A. L.; Herdies, D. L.; Alvim, D. S.; Vendrasco, É. P.; Figueroa, S. N.; Pendharkar, J.; Reyes Fernandez, J. P. A new predictive framework for Amazon forest fire smoke dispersion over South America. *Bull. Am. Meteorol. Soc.* **2021**, *102*, E1700−E1713.
(53) Cuesta, J.; Eremenko, M.; Liu, X.; Dufour, G.; Cai, Z.; Höpfner, M.; von Clarmann, T.; Sellitto, P.; Foret, G.; Gaubert, B.; Beekmann, M.; Orphal, J.; Chance, K.; Spurr, R.; Flaud, J.-M. Satellite observation of lowermost tropospheric ozone by multispectral synergism of IASI thermal infrared and GOME-2 ultraviolet measurements over Europe. *Atmos. Chem. Phys.* **2013**, *13*, 9675−9693.
(54) Cuesta, J.; Kanaya, Y.; Takigawa, M.; Dufour, G.; Eremenko, M.; Foret, G.; Miyazaki, K.; Beekmann, M. Transboundary ozone pollution across East Asia: daily evolution and photochemical production analysed by IASI + GOME2 multispectral satellite observations and models. *Atmos. Chem. Phys.* **2018**, *18*, 9499−9525.
(55) Guenther, A.; Karl, T.; Harley, P.; Wiedinmyer, C.; Palmer, P. I.; Geron, C. Estimates of global terrestrial isoprene emissions using MEGAN (Model of Emissions of Gases and Aerosols from Nature). *Atmos. Chem. Phys.* **2006**, *6*, 3181−3210.
(56) Draxler, R. R. Demonstration of a global modeling methodology to determine the relative importance of local and long-distance sources. *Atmos. Environ.* **2007**, *41*, 776−789.
(57) Stein, A. F.; Isakov, V.; Godowitch, J.; Draxler, R. R. A hybrid modeling approach to resolve pollutant concentrations in an urban area. *Atmos. Environ.* **2007**, *41*, 9410.
(58) Thalman, R.; de Sá, S. S.; Palm, B. B.; Barbosa, H. M. J.; Pöhlker, M. L.; Alexander, M. L.; Brito, J.; Carbone, S.; Castillo, P.; Day, D. A.; Kuang, C.; Manzi, A.; Ng, N. L.; Sedlacek, A. J., III; Souza, R.; Springston, S.; Watson, T.; Pöhlker, C.; Pöschl, U.; Andreae, M. O.; Artaxo, P.; Jimenez, J. L.; Martin, S. T.; Wang, J. CCN activity and organic hygroscopicity of aerosols downwind of an urban region in central Amazonia: seasonal and diel variations and impact of anthropogenic emissions. *Atmos. Chem. Phys.* **2017**, *17*, 11779−11801.
(59) Xing, J.; Wang, J.; Mathur, R.; Wang, S.; Sarwar, G.; Pleim, J.; Hogrefe, C.; Zhang, Y.; Jiang, J.; Wong, D. C.; Hao, J. Impacts of aerosol direct effects on tropospheric ozone through changes in atmospheric dynamics and photolysis rates. *Atmos. Chem. Phys.* **2017**, *17*, 9869−9883.
(60) Forkel, R.; Balzarini, A.; Baró, R.; Bianconi, R.; Curci, G.; JiménezGuerrero, P.; Hirtl, M.; Honzak, L.; Lorenz, C.; Im, U.; Pérez, J. L.; Pirovano, G.; San José, R.; Tuccella, P.; Werhahn, J.; Žabkar, R. Analysis of the WRF-Chem contributions to AQMEII phase2 with respect to aerosol radiative feedbacks on meteorology and pollutant distributions. *Atmos. Environ.* **2014**, *115*, 630.
(61) Kong, X. Analysis of meteorology−chemistry interactions during air pollution episodes using online coupled models within AQMEII phase-2. *Atmos. Environ.* **2015**, *115*, 527−540.
(62) Vara-Vela, A.; de Fátima Andrade, M.; Zhang, Y.; Kumar, P.; Ynoue, R. Y.; Souto-Oliveira, C. E.; da Silva Lopes, F. J.; Landulfo, E. Modeling of atmospheric aerosol properties in the São Paulo metropolitan area: Impact of biomass burning. *J. Geophys. Res.: Atmos.* **2018**, *123*, 9935−9956.
(63) Liu, L.; Cheng, Y.; Wang, S.; Wei, C.; Pöhlker, M. L.; Pöhlker, C.; Artaxo, P.; Shrivastava, M.; Andreae, M. O.; Pöschl, U.; Su, H. Impact of biomass burning aerosols on radiation, clouds, and precipitation over the Amazon: relative importance of aerosol−cloud and aerosol−radiation interactions. *Atmos. Chem. Phys.* **2020**, *20*, 13283−13301.